Remote Sens. **2014**, *6*, 11731-11752; doi:10.3390/rs61211731

OPEN ACCESS

remote sensing

ISSN 2072-4292

www.mdpi.com/journal/remotesensing

Article

Quantifying the Physical Composition of Urban Morphology throughout Wales Based on the Time Series (1989–2011) Analysis of Landsat TM/ETM+ Images and Supporting GIS Data

Douglas Scott [1,*], George P. Petropoulos [1], Janet Moxley [2] and Heath Malcolm [2]

[1] Department of Geography & Earth Sciences, Aberystwyth University, Llandinam Building, Penglais Campus, Aberystwyth, SY23 3DB, Wales, UK; E-Mail: george.petropoulos@aber.ac.uk

[2] Centre for Ecology and Hydrology, Bush Estate, Penicuik, Midlothian, EH26 0QB, Scotland, UK; E-Mails: janmox@ceh.ac.uk (J.M.); hmm@ceh.ac.uk (H.M.)

* Author to whom correspondence should be addressed; E-Mail: douglasscotteo@gmail.com; Tel.: +44-0-1970-621861.

External Editors: Janet Nichol and Prasad S. Thenkabail

Received: 16 July 2014; in revised form: 28 October 2014 / Accepted: 30 October 2014 / Published: 25 November 2014

Abstract: Knowledge of impervious surface areas (ISA) and on their changes in magnitude, location, geometry and morphology over time is significant for a range of practical applications and research alike from local to global scales. Despite this, use of Earth Observation (EO) technology in mapping ISAs within some European Union (EU) countries, such as the United Kingdom (UK), is to some extent scarce. In the present study, a combination of methods is proposed for mapping ISA based on freely distributed EO imagery from Landsat TM/ETM+ sensors. The proposed technique combines a traditional classifier and a linear spectral mixture analysis (LSMA) with a series of Landsat TM/ETM+ images to extract ISA. Selected sites located in Wales, UK, are used for demonstrating the capability of the proposed method. The Welsh study areas provided a unique setting in detecting largely dispersed urban morphology within an urban-rural frontier context. In addition, an innovative method for detecting clouds and cloud shadow layers for the full area estimation of ISA is also presented herein. The removal and replacement of clouds and cloud shadows, with underlying materials is further explained. Aerial photography with a spatial resolution of 0.4 m, acquired over the summer period in 2005 was used for validation purposes. Validation of the derived products indicated an overall ISA detection accuracy in

the order of ~97%. The latter was considered as very satisfactory and at least comparative, if not somehow better, to existing ISA products provided on a national level. The hybrid method for ISA extraction proposed here is important on a local scale in terms of moving forward into a biennial program for the Welsh Government. It offers a much less subjectively static and more objectively dynamic estimation of ISA cover in comparison to existing operational products already available, improving the current estimations of international urbanization and soil sealing. Findings of our study provide important assistance towards the development of relevant EO-based products not only inaugurate to Wales alone, but potentially allowing a cost-effective and consistent long term monitoring of ISA at different scales based on EO technology.

Keywords: Wales; Landsat; impervious surface estimation; multi-temporal imagery; object-orientated method

1. Introduction

In 2011, it was recorded that around half of the World's population (~3.5 billion people) were living in urban environments [1]. Impacts of this growth and urban expansion over the last century have been the loss of fertile and otherwise green-space to concrete for ever increasing areas of housing and infrastructure. The covering of land with impervious surfaces (*i.e.*, roads, pavements, buildings, and other concreted areas) seals the soil and prevents many essential ecosystem services: the production of food; habitat for plants; micro climate regulation. The quantifiable amount of these impervious surface areas (ISA) is therefore considered extremely important in a context of monitoring climate change. As a mark of their importance, the United Nations Framework Convention on Climate Change (UNFCCC) have requested information on ISA figures, from all members states, to be included amongst other significant land use categories for submission into the Greenhouse Gas Inventory for the years 1990–2011 [2]. As a result of this, the EU also demands accurate figures for feeding in to the Greenhouse Gas Inventory.

Others, e.g., [3], identify ISA as a key environmental indicator. ISAs are defined mainly as artificial structures and surfaces, such as buildings, pavements and car parks that do not allow the downward transfer of water and therefore prevent the ecological services of the underlying soil. Thus, those are one of the main contributors to environmental degradation [4]. Because increases in ISA's are often indicative of urban and industrial development, they are also one of the main indicators of urbanisation and urban sprawl [5,6]. With the World's urban population only predicted to grow and expand into an ever dwindling green environment [7], and given the environmental impacts, it is evidently a key requirement nowadays to quantify global ISA's in a cost-effective and consistent manner.

Earth Observation (EO) technology provides an economically effective solution, has the potential to be more accurate than traditional mapping methods, and can be instantaneously adapted given dynamic objectives. The capability of EO technology for large scale operational application and the plethora of additional EO datasets available, make it an appropriate solution to mapping ISAs [8,9]. Image classification is the most commonly applied approach in deriving spatially distributed maps of land use

and land cover [10–12]. Many methods have been developed for extracting ISA from EO imagery, a comprehensive review of which can be found in [13]. While pixel-based classifications have long been utilized to interpret landscapes and distinguish between habitats, segmentation techniques in combination with object-based image analysis (OBIA) provide information on targets according to shape, spectral difference and a variety of user defined variables [9]. Due to the salt and pepper effect prominently created by a pixel-based classification approach [14], OBIA is generally considered to produce results that are much easier to subsequently manipulate in a Geographical Information Systems (GIS) environment. Results produced by OBIA are then much easier to understand and visually interpret in comparison to pixel-based methods. By virtue of this, OBIA has been documented to improve the accuracy of classifications by around 2–3% [15–18], or more [6,8,19] compared to per-pixel techniques. Examples of studies that utilize OBIA for the extraction of urban features are legion. However, it has been suggested that while OBIA is useful for image classification, it should be utilised only for masking of other non-target materials, such as vegetation and water; therefore creating a fusion technique of OBIA and sub-pixel analysis [20].

The detection of ISA's using EO data has also aided the modelling of rainfall-runoff in the field of urban hydrology [21–23] and prediction [24]. Many of the most prolific studies on ISA EO research have focused on large urban settlements in the USA and China [19,25–27]. A relatively small number of studies have also been concerned in exploiting EO technology for urban land-use studies in the United Kingdom (UK) as well [28–31]. For example, the first study of its kind in the UK; [28] used SPOT HRV data to monitor "urban encroachment" in south-east. Authors concluded that the application of EO imagery and derived land-use detection techniques for rural-urban change in the UK was valuable and promising option. However, another 14 years passed before the next EO-based urban study was published [30]. In this work, authors used radar data from the ESA's ERS satellite to map urban change. This study focused on the UK and more specifically in Cardiff, the capital of Wales. While [29] used Landsat TM data to produce a land-use map for the UK, ISA surfaces were still not the main focus of these authors' study. Therefore, the need for an accurate up-to-date estimate of urban land cover composition in Wales and other EU member states is prolific, especially when the current EU standing on impervious surfaces, is considered.

Cloud-free EO imagery is useful for time-series analysis due to homogeneity in spectral signatures across given study areas and therefore the classification of general land cover types [32]. However, access to cloud-free imagery is either difficult or in some cases nearly impossible for an entire country if located near the poles. A variety of image processing methods have been proposed in detecting clouds from EO imagery [33–37]. Many methodologies have been presented to remove these clouds and their derived shadows, the most ingenious of which are based on sun illumination angle, topography, and cloud elevation [32,38–40]. Clouds are common across the Welsh coast due to Atlantic depressions, forming a large proportion of the showers and thunderstorms that are characteristic of the region. This makes the acquisition of cloud-free imagery for the whole country a challenging task, if not near-impossible and thus methods similar to the formerly discussed have to be employed.

Obtaining high resolution EO data is sometimes not an option due to budgetary and other constrains. Freely distributed EO data in these cases are preferred. However, freely available data are often of a much coarser resolution than more expensive counterparts. The impediment of coarse/medium resolution imagery is that of mixed pixels. In order to extract impervious surface cover from

coarse/medium resolution imagery, many studies have been based on sub-pixel analysis techniques [5,41–47]. Linear spectral mixture analysis (LSMA) is a method of sub-pixel analysis often employed in studies using medium or coarse resolution multi- and also when hyper-spectral data is available. Producing a user-defined number of fractional images this method has proven valuable for extracting ISAs being able in particular to separate them from spectrally similar materials such as soil. The most common example of imagery used for this analysis is that of the Landsat series [43,45,47]. The LSMA approach assumes that the spectral information measured by the receiving sensor is mixed in a linear combination of the spectra of all components. These components are otherwise known as end-members. [48] assumed that the urban landscape was composed of three main materials; vegetation, soil and impervious surfaces. In order to attain a more accurate representation of the urban landscape from EO data, contemporary studies [46,49,50] use four end-members including vegetation, high-albedo, low-albedo and soil. The high-albedo fraction highlights surfaces with high spectral reflection such as bright impervious surfaces, while the low-albedo fraction highlights dark impervious surfaces. This method is generally considered superior to that of Normalized Difference Indexes (e.g., NDXI, [19]) due to the user-defined selection of training samples. Although this requires more user input and therefore project time, the result is often superior and is therefore utilised regularly across the literature [19].

Currently existing products for extracting ISA in the UK include:

- The Phase 1 habitat survey [51,52], the primary spatial dataset for lowland and upland habitats in Wales and the UK.
- The Ordinance Survey (OS) MasterMap product, the most prolific and contemporary GIS-based boundary dataset in the UK [53,54].
- The National Land Use Database (NLUD), developed by the Geoinformation group and providing a national set of predefined land-use polygons [55].
- The "imperviousness" high resolution layer form the Copernicus Land Monitoring Service; a simple inversion of NDVI. Attempts have been made to improve the methodology [56,57].
- Finally, the Coordinated Information on the European Environment (CORINE) land cover map, which is part of a European objective for monitoring land use across Europe.

These products, available to the UK scientific community for land-use and therefore deriving land-use change such as ISA, are insufficient in their construction and accuracy. They cater for subjectively static rather than objectively dynamic project interrogation of land-use materials and serve only as a useful boundary resource. Given the present EU focus on soil sealing and impervious surfaces, alternative data must be developed. Although this has been attempted by Copernicus Land Services, this service is not being planned to be widely distributed until 2015 and currently only covers the years 2000–2012, rather than the inventory years of 1990–2011. Over an area as large as Wales, traditional survey techniques are no longer viable and therefore EO technologies must be endorsed.

In preview of the above, the present study was aimed at proposing a new GIS/EO data hybrid method for the extraction and estimation of ISA concentration and demonstrates the applicability of this technique over selected study sites in Wales, UK. The study also demonstrates the use of an innovative method for mapping and masking clouds and cloud shadows [32].

2. Study Sites and Datasets

2.1. Study Sites

Based on growth rank from statistics on new builds provided by the Welsh Government, study sites were selected to provide a broad representation of Wales. The statistics roughly cover the temporal scale (1990–2012) of the study and Green House Gas inventories model [2]. Based on these statistics, the unitary authorities of Cardiff, Swansea, Rhondda Cynon Taf, Caerphilly, Wrexham, Neath Port Talbot and Aberystwyth (Figure 1) were chosen. The major concentration of population and industry in Wales is in the five contiguous study sites of South Wales (Cardiff, Swansea, Rhondda Cynon Taf, Caerphilly and Neath Port Talbot). It is therefore imperative that ISA's in these areas, including the capital Cardiff are quantified for the Green House Gas inventories.

Figure 1. Map showing the distribution of our study areas (shown in yellow color) across Wales.

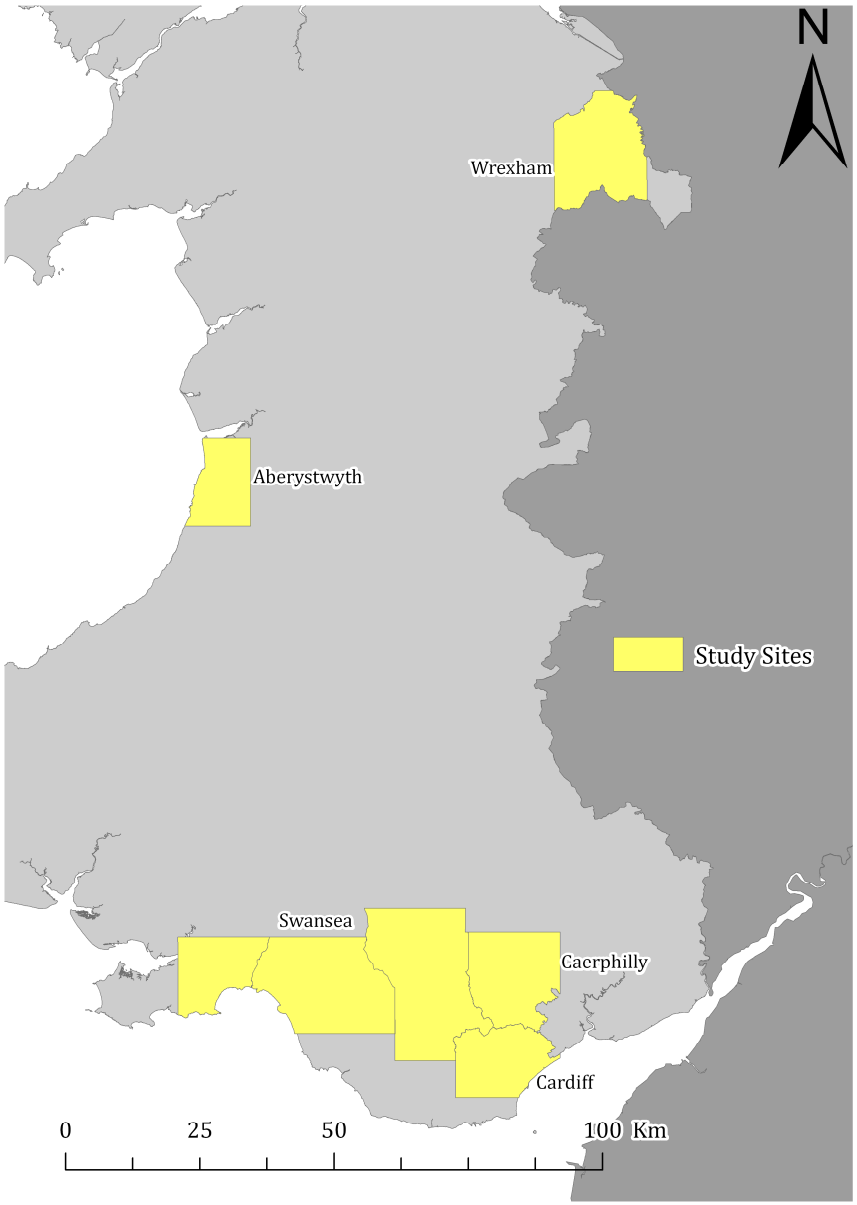

The town of Aberystwyth in particular has increased dramatically in size over the past two decades due to the sale of agricultural land located to the east of the main town centre. From expert local knowledge, this has included the development of a large commercial estate and two housing estates. The Wrexham study area is within North Wales which contains the Snowdonia national park to the North. A large quarry, of which the main material is bare earth, which often provides a strong obstacle in ISA research and extraction also resides to the north of the town centre.

2.2. Datasets

To satisfy the objectives of this study, freely distributed EO imagery and a digital terrain model (DEM) were acquired. This dataset included 13 Landsat TM and ETM+ scenes of varying levels of cloud cover, supplied by the United States Geological Survey (USGS). The main criteria for selecting scenes were closest to 0% cloud cover within the primary leaf-on season (UK summer period, July–September), allowing the most recorded reflectivity possible [19,58]. Scenes from the primary leaf-on season that were partially—fully covered in cloud were replaced by scenes from other dates within the same year with closest to 0% cloud cover (Table 1). In addition, a mosaicked coverage of DEM data at a spatial resolution of 5 m, supplied by NEXTMap (a local Welsh company) was also utilised.

In addition to the Landsat scenes, aerial photography coverage for all study sites, acquired over the summer period of 2006 with a spatial resolution of 40 cm (captured by COWI and supplied by the Welsh Government) was used to assess the performance of the ISA estimation. To further assess, in part the accuracy of the classification and in part the inadequacy of the currently existing GIS-based products for ISA estimation, the OS MasterMap product was used. Details of this dataset are referred to in the works of [53,54,59].

Table 1. Landsat data acquired for the classification and estimation of impervious surface areas (ISA) concentration.

Sensor	Path	Row	Date
Landsat-5 TM	204	23	10 February 1989
Landsat-5 TM	204	23	28 April 1989
Landsat-5 TM	204	24	28 April 1989
Landsat-7 ETM+	204	23	24 July 1999
Landsat-7 ETM+	204	24	24 July 1999
Landsat-7 ETM+	204	23	10 September 1999
Landsat-7 ETM+	204	24	10 September 1999
Landsat-7 ETM+	204	23	13 March 2003
Landsat-7 ETM+	204	24	13 March 2003
Landsat-7 ETM+	203	23	22 March 2003
Landsat-7 ETM+	203	24	22 March 2003
Landsat-5 TM	204	23	28 April 2011
Landsat-5 TM	204	24	28 April 2011

3. Methodology

3.1. Data Pre-Processing

In order to compensate for inter-platform gains and bias difference and to therefore enable multi-temporal comparisons, an absolute atmospheric correction method was required. Visibility data was therefore needed as an input for the atmospheric correction models utilized with the fast line-of-sight atmospheric analysis of spectral hypercubes (FLAASH) module developed in ENVI [60,61]. This data was supplied by the met office integrated data archive system (MIDAS) stations situated around the country. To mask out all known 0% ISA's, the land parcel identification system (LPIS) [62] was used in conjunction with extracted water layer from the OS MasterMap product (Technical specification available at: http://www.ordnancesurvey.co.uk/docs/user-guides/os-mastermap-topography-layer-user-guide.pdf).

3.2. ISA Extraction

The process tree for the classification and estimation of ISA (Figure 2) was built on the basis of a multiple part classification, similar to that of a hierarchal segmentation [58]. Each progressive part acted as a mask for its subordinate and refined the impervious surface estimation area further. Part I provided simple integration of the existing data layers, Part II produced the classification of remaining 0% impervious surface features, and Part III estimated the ISA from 1–100% (Figure 3) Parts I and II were implemented using an OBIA approach to classification while Part III was performed separately in the ENVI platform to enable sub-pixel analysis for ISA estimation.

Part I of the process tree integrated the existing GIS data layers to mask known 0% ISA's from the rest of the scene. Areas deemed physically impossible or unlikely to host large ISA's areas > 20% slope were also removed. This utilised the DTM for areas above an altitude of 350 m.a.s.l., as suggested by [58], for the South Wales and Wrexham study areas, and areas above 300 m.a.s.l. for the Aberystwyth study area; these varied in height due to the employment of expert local knowledge from the author and colleagues from the Welsh Government. Remaining areas were then interrogated for the existence of areas above an average slope of 20°. Using OS MasterMap data, the high tide lines (for coastal study sites) and inland water bodies (for all study sites) were masked out of the rest of the scene. LPIS polygon data, supplied by the Welsh Government were then utilized to mask out areas of known agriculture.

By virtue of the general climate of Wales and the return periodicity of the Landsat satellites, it was not constantly possible to obtain optical data for cloud-free summer dates. A further series of sub-routines in Part I of the process were therefore required in order to assess the need for alternative data. Clouds and associated shadows were detected in scenes by utilising the innovative method first presented in [32]. This approach required measurements taken by the Landsat satellite at the time of acquisition as well as averaged user derived measurements from corresponding points on selected cloud and shadow. When alternative data was required over the entire scene winter season images were utilized. An assessment of acquisition time solar azimuth derived topographic shadow was therefore required and used to once again assess the need for further alternative data.

Figure 2. Flow chart showing the methods of pre-processing, classification, and validation in the present study, where image processing and classification; Part I is the simple classification and alternative data sub-setting, Part II is the advanced classification of remaining objects and the use of alternative data, and Part III is the linear spectral mixture analysis. Post classification analysis Part I is the comparison between the user classification and OS MasterMap, and Part II is the concentric circle analysis and comparison between the user classification and the aerial photography.

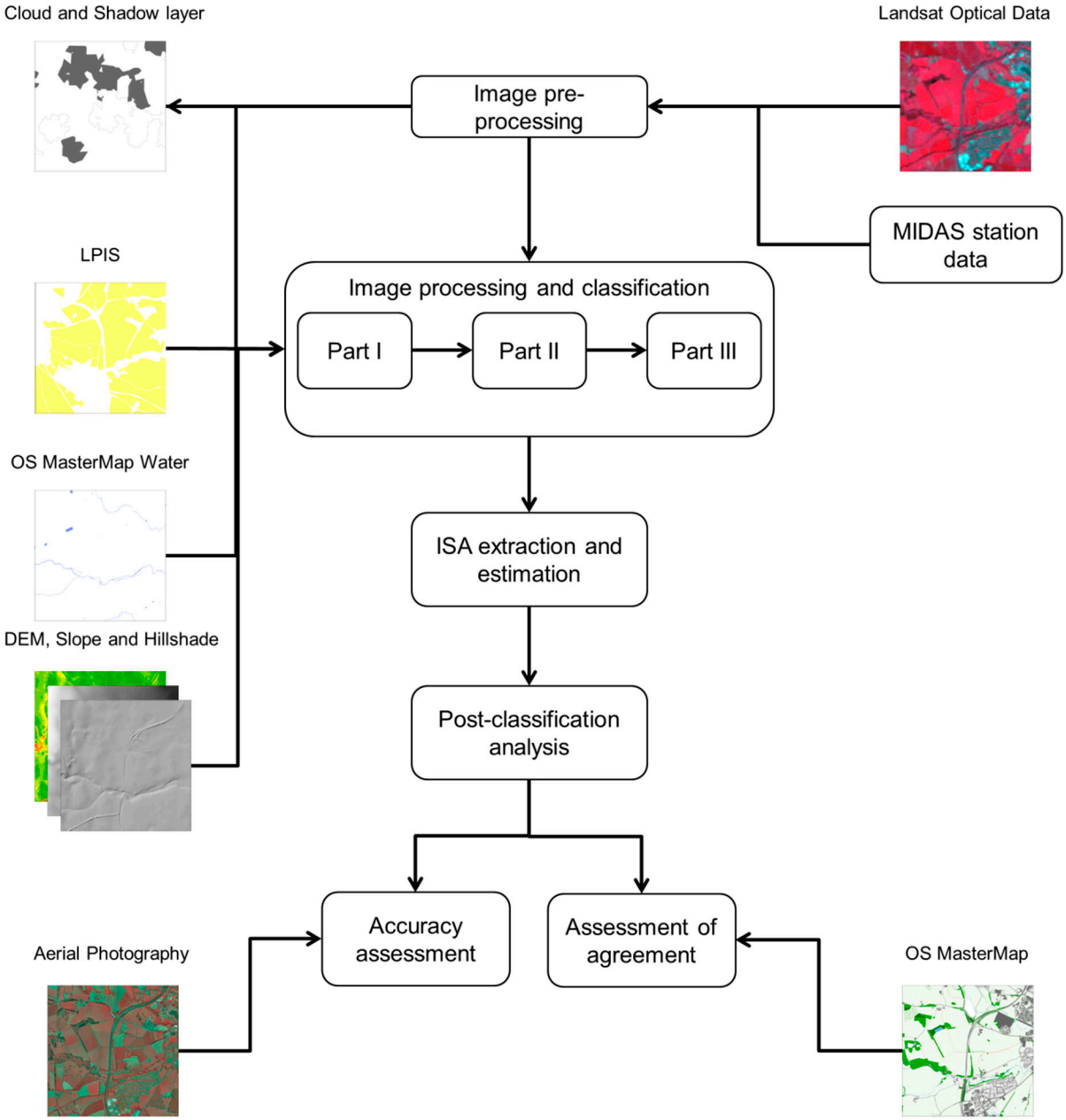

Figure 3. The hierarchal parts of the methodology where: Part I (**top**), a simple masking of all known 0% ISA's; Part II (**middle**), further masking of vegetation and bare earth features; and Part III (**bottom**) extraction and estimation of ISA's in the remaining urban areas.

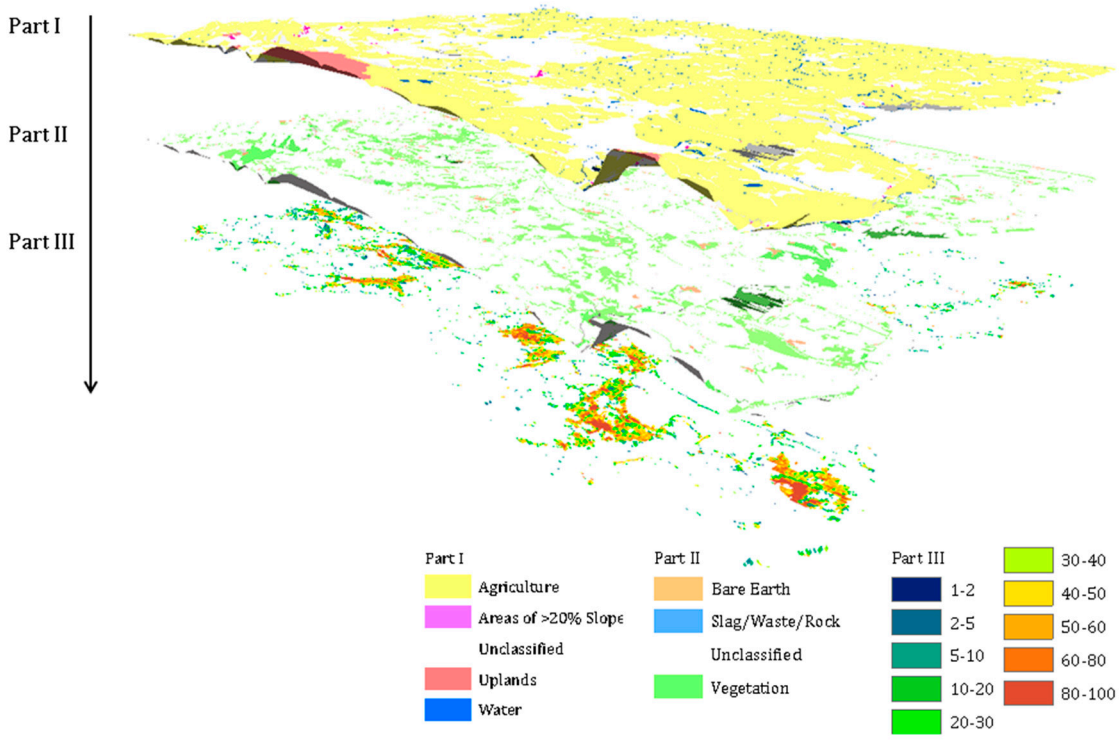

To assess the alternative data based on cloud and shadow, Part II of the process tree was firstly split into two sets of parallel sub-routines:

- Spectral thresholding for the primary data in summer seasons
- Spectral thresholding for the alternative data in other seasons

Both of these parallel sub-routines involved the extraction of any vegetation that was not masked out within Part I and the extraction of bare earth and rock features from the scene. While the extraction of the former areas presents itself as a relatively simple task, extraction of the latter is not. Each scene was therefore individually analysed for the unique spectral signatures of known bare earth and rock features which lye spectrally between low density urban and high density urban features, and generally cover a large uniform area, such as quarries and slag piles. These are characteristic of the more industrialized sites and therefore made a significant contribution to the final output.

Finally, Part III of the process tree involved the estimation of ISA coverage from the remaining areas, not masked by Parts I and II. Following the principals of [48] and later, [63], remaining pixels were estimated as a linear mixture of three principal materials; vegetation, ISA and soil. The V-I-S model can also be expressed as the linear mixture model [64]:

$$R_u = \sum_{j=1}^{n} \left(r_i f_{uj} + e_u \right) \quad (1)$$

where R_u is the reflectance of pixel u; r_j is the spectral reflectance of surface component j; f_{uj} is the fraction of surface component j in pixel u; e_u is the un-modeled residual for pixel u; and n is the number of surface components.

These were split according to the Biophysical Composition Index (BCI), first proposed by [63], involving the post-processing of the Landsat optical data by examination and inclusion of the Tasseled Cap (TC) transformation, originally developed for Landsat 5 MSS imagery, by [65] and later for Landsat 7 ETM+ imagery by [66].

$$BCI = \frac{(H + L)/2 - V}{(H + L)/2 + V} \tag{2}$$

where H is "high albedo", the normalized TC1; L is "low albedo", the normalized TC3; and V is "vegetation", the normalized TC2. These are therefore normalized in the following formula that:

$$H = \frac{TC1 - TC1_{min}}{TC1_{max} - TC1_{min}} \tag{3}$$

$$V = \frac{TC2 - TC2_{min}}{TC2_{max} - TC2_{min}} \tag{4}$$

$$L = \frac{TC3 - TC3_{min}}{TC3_{max} - TC3_{min}} \tag{5}$$

3.3. Validation

3.3.1. Accuracy Assessment

In order to review the accuracy of the classification, platform supplied error matrices have traditionally been used [67,68]. However, the more traditional forms of error and confusion matrices to assess the accuracy of classification were judged too simplistic [69]. Alternative methods that use a concentric circle concept upon which sample plots are drawn in the eight cardinal directions have been presented in more contemporary literature [13,70,71]. Herein was followed this guideline and 10 × 10 pixel (300 m × 300 m) plots were randomly selected to cover all study areas. The classification results were converted from WGS 1984 UTM zone 30N to British National Grid to make the coordinate system consistent with the aerial photography. The plots were selected based on the intersection of straight lines, following the eight cardinal directions (N, NE, E, SE, S, SW, W, NW), and concentric circles, with a distance of 100 pixels (3000 m) between two circles, from the centroid, to the extreme of each study area. Due to the 2-year gap between the Landsat ETM+ data (2003) and the geo-referenced ortho-rectified aerial photography (2005), a careful inspection was conducted based on expert local knowledge of the study areas. Where problems were detected, the plots were replaced with another randomly selected plot, drawn from a random sampling tool available in ArcGIS. The LSMA was modified by the results of Parts I and II of the classification and average values were extracted from each of the plots. An unsupervised *Nearest Neighbour* classification was performed on the corresponding areas of the aerial photography and ISA's identified and averaged across individual plots. From these two results, the root mean square error (RMSE), the mean absolute error (MAE), and the coefficient of determination (R^2), between the ISA's in both datasets were calculated, using Microsoft Office Excel. The formulae are given below:

$$RMSE = \sqrt{\frac{\sum_{i=1}^{N}(\hat{I} - I_i)^2}{N}} \quad (6)$$

$$MAE = N^{-1}\sum_{i=1}^{N}\left|I_i - \hat{I}_i\right| \quad (7)$$

$$R^2 = \frac{\sum_{i=1}^{N}\left(\hat{I}_i - \bar{I}_i\right)}{\sum_{i=1}^{N}(I_i - \bar{I}_i)^2} \quad (8)$$

where $\hat{I}i$ is the estimated ISA fraction for sample i; Ii is the ISA proportion calculated from the unsupervised classification of the aerial photography; $\bar{I}$ is the mean value of the samples; and N is the number of samples [6].

3.3.2. Assessment of Agreement

In our study, a quantitative comparison between the classification results and the OS MasterMap product was firstly performed in order to assess the appropriateness of the currently most widely used GIS product on the UK for the purposes of ISA extraction. A technique first employed for assessing the accuracy of calculated burn scar areas [17,72,73] was utilised to detect the efficiency of the user classification compared to the ISA's outlined by the OS MasterMap product. In order to carry out this accuracy assessment, it was necessary to derive three parameters from the user classification and the OS MasterMap product and input into three separate formulae. These included the Detected Area Efficiency (DAE), False Area Rate (FAR, commission error) and the Skipped Area Rate (SAR, omission error), which were derived from the following equations:

$$DAE = \frac{DIA}{DIA + SIA} \quad (9)$$

$$FAR = \frac{FIA}{DIA + FIA} \quad (10)$$

$$SAR = \frac{SIA}{DIA + SIA} \quad (11)$$

where: *DIA* is the detected impervious area (common area between the generated impervious area dataset by the proposed method application and the reference OS MasterMap), *SIA* is the skipped impervious area (the area included in the OS MasterMap but not in the generated impervious area dataset by the proposed method application), and *FIA* is the false impervious area (the area included in the generated impervious surface area by the proposed method application but not in the OS MasterMap). DAE, FAR and SAR take values between 0 and 100%, where values greater than 80% represent generally a very good agreement between by the impervious surface area predicted by the proposed method application and reference MasterMap dataset [72,73]. This step was performed in ArcGIS software platform (ESRI Inc., v. 10.1)

4. Results

The three part classification process method quantified the sub-pixel fractions of high albedo, vegetation and low albedo; as described in [63]. Figures 4 and 5 show the results of the masking and

subsequent estimation of ISA's, in Wrexham and the South Wales study sites. A large fraction of ISA's are distributed within the city centres and satellite industrial areas; medium fractions of ISA's are distributed amongst the residential areas of towns and cities within the all study area; and agricultural areas (the largest land cover type in Wales) that were not masked by Parts I or II (arable and non-arable), have an extremely low fraction of ISA. The largest changes in all study areas occurred during the 1990s (1989–1999). While the net urban area increased consistently at variable amounts, ISA fractions increased toward the middle of the study period and subsequently decreased at the end of the study period, with period-end values still higher than the original period-start values. The largest study area percentage coverage of ISA's was found in the Welsh capital Cardiff. However, the largest mean values of ISA fractions over single study areas occur in the major industrial areas of South Wales, fluctuating between ~64% and 55% from 1989–2011 and Wrexham, north Wales, fluctuating between 70% and 63% from 1989 to 2011.

The accuracy of the three part classification process method by comparing its results to high resolution aerial photography (supplied by the Welsh Government) was also evaluated. Figure 6 shows the accuracy assessment of ISA estimated by our proposed approach. A greater number (98 out of 144) of assessment plot windows were located within the five contiguous South Wales study areas due to the large area percentage (73%) of the entire study represented. There was some overestimation in the lower percentages of ISA and a small number of underestimated plots in the higher percentages of ISA estimation. However, this still resulted in an r^2 value of 0.95 with an RMSE of 0.054.

Figure 4. ISA extraction from the contiguous South Wales study sites for; 1989 (**top left**), 1999 (**top right**), 2003 (**bottom left**), and 2011 (**bottom right**).

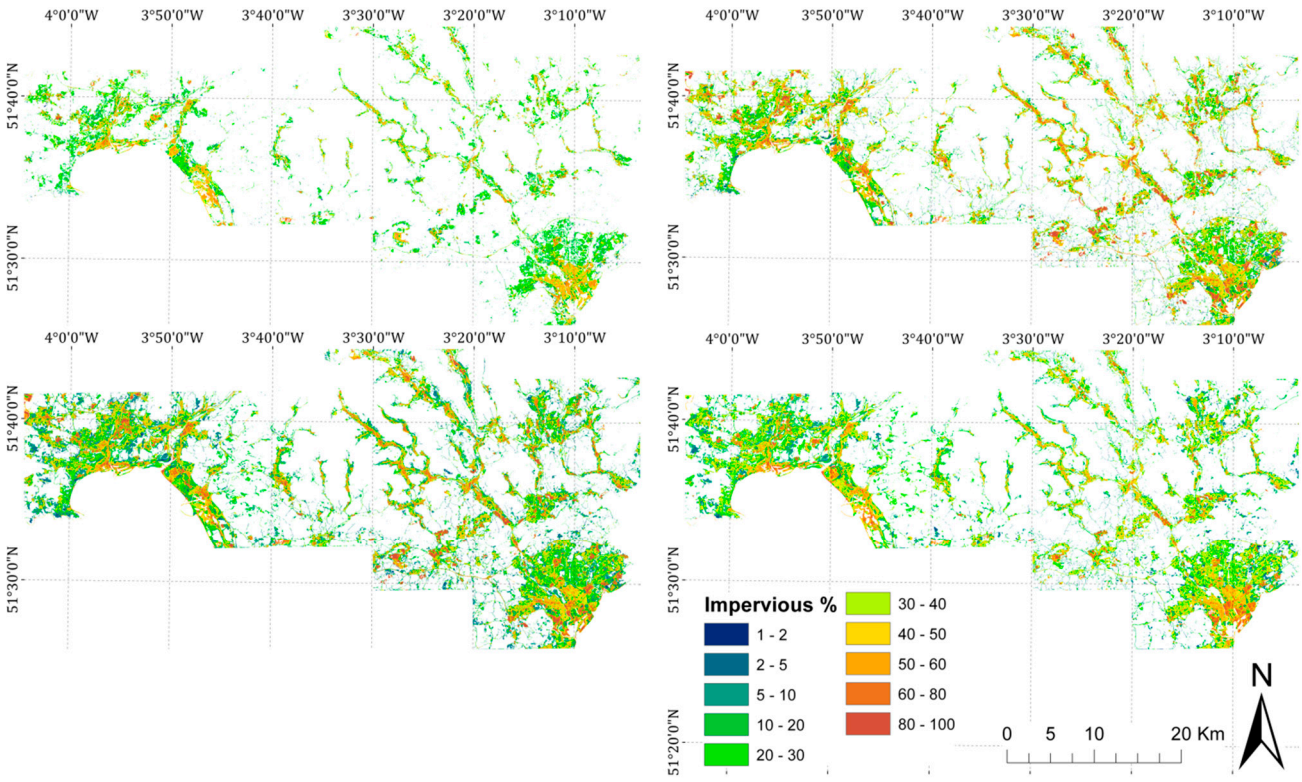

Figure 5. ISA extraction over the Wrexham study area for 1989 (**top left**), 1999 (**top right**), 2003 (**bottom left**), and 2011 (**bottom right**).

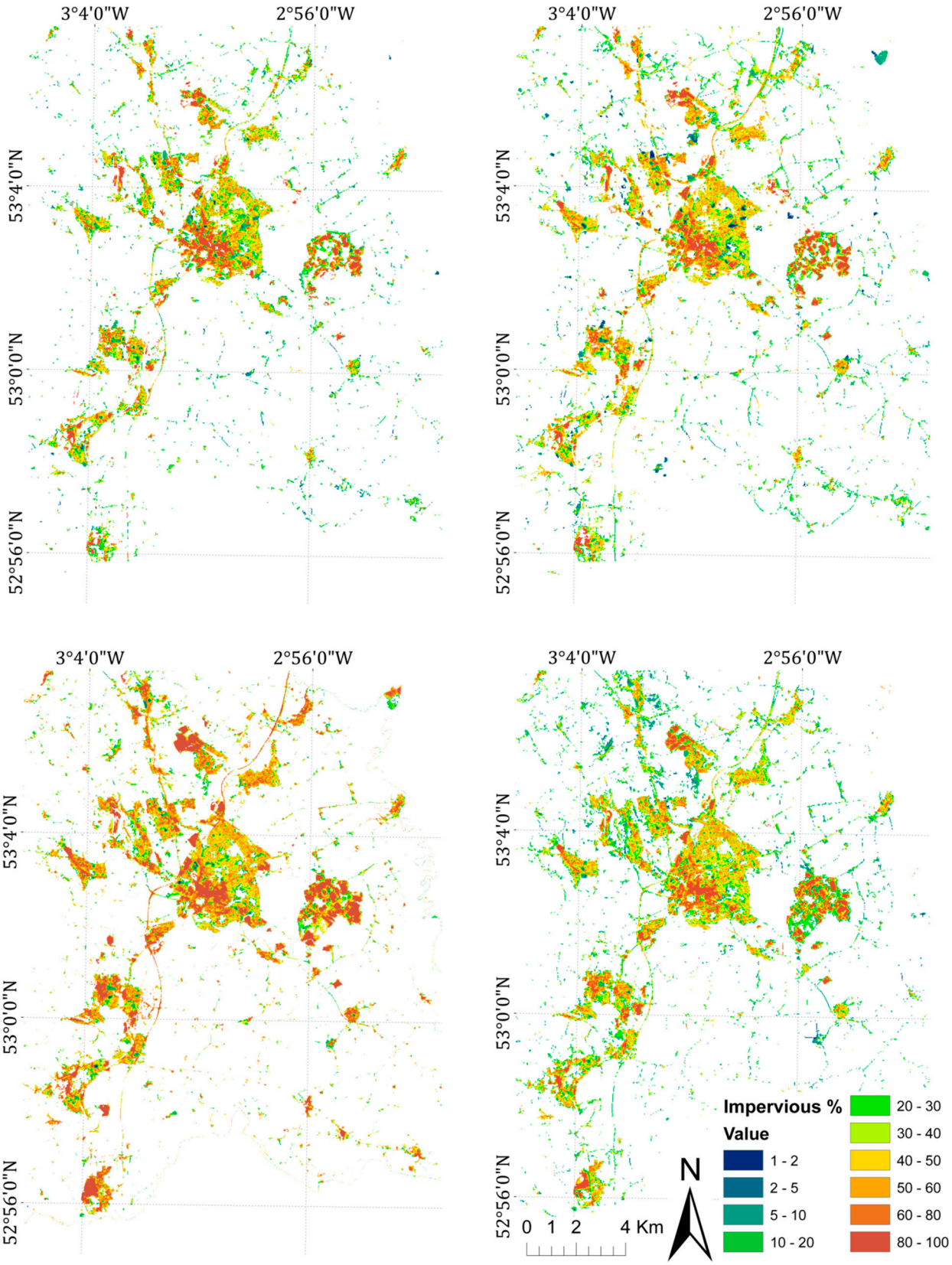

Figure 6. Accuracy assessment of extracted ISA in comparison to high resolution aerial photography, (over 144 sample plots) where the grey line represents a 1:1 ratio and the black is the linear trend line.

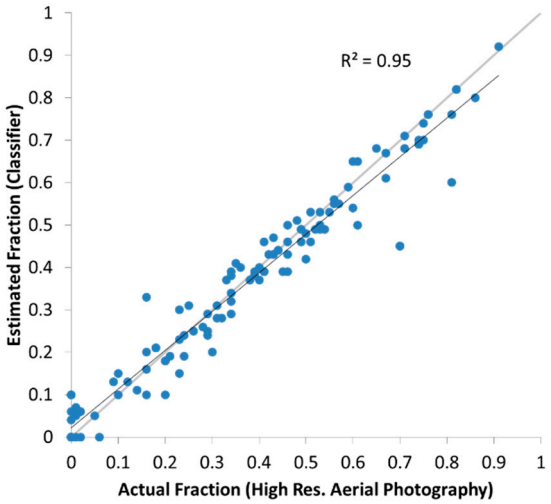

In order to assess the appropriateness of utilizing OS Master Map for the extraction of ISA within the UK, as is currently done, a number of scores were generated for all the seven study areas selected for the 2011 results, following [72,73]. The DAE's were highly variable between study areas with only 21% for Wrexham and 85% for Swansea. Average scores for the seven study areas were 62%, 37% and 61% for DAE, SAR and FAR respectively (Table 2).

Table 2. Detected Area Efficiencies (DAE), False Area Rates (FAR), and Skipped Area Rates (SAR), converted to percentage scores; for all seven study sites in 2011, when compared to OS MasterMap.

Study Site	DAE	SAR	FAR
Wrexham	21.67	78.33	62.49
Aberystwyth	58.10	41.90	66.42
Swansea	86.12	13.88	59.26
Neath Port Talbot	78.61	21.39	63.69
Rhondda	77.08	22.92	60.23
Caerphilly	72.65	27.35	61.59
Cardiff	46.64	53.36	54.75
Average	62.98	37.02	61.20

5. Discussion

5.1. Analysis of Dynamic Changes in ISA

ISA expansion can be easily observed both visually and quantitatively across the South Wales study sites (Figure 4). Average concentrations of ISA within the urban extent increased from 1989 to 2011 with a peak of ISA in 1999. This peak correlates with a housing development "boom" that occurred in 1999 [30] in the UK with many housing developments being commissioned across the UK, while the

relative lulls of 1989 and 2011 also coincide with the beginning of economic recession. The reflection of this in the results presented is therefore information of high priority to sustainable planning and urban management. While the outer extents of many of the urban areas in Wales have not altered significantly over the past 22 years, the ISA within them has significantly expanded. This would therefore suggest that policies on urban restriction have led to the infilling of existing urban boundaries [74] and the green spaces within them in order to accommodate expanding populations.

5.2. Comparisons with OS MM

Figure 7 shows comparisons between the results of the proposed method and the OS MM product in selected sample locations. This highlights the lack of detail in residential areas of the OS MM product, with around 80% of the falsely classified areas being gardens. With private land use changing fairly frequently, responsive with social and financial trends, it would seem important to track these changes in terms of ISA [30]. The OS MasterMap product may not ever hope to do this as the main remit of the product is to identify land parcels rather than materials [54,75]. Under normal circumstances, high *FAR* scores would be indicative of a poor classification but this is on the contrary here due to the lack of detail in residential areas for the OS MM product. This is reflected in Table 2, with the false area rates often exceeding 50%. With minimal effort compared to manually digitising many different materials within all urban environments, the classifier has proven capable of quantifying these variables.

Figure 7. Comparison of extracted ISA between **a**, **b**, **c**: high resolution aerial photography (for reference), **d**, **e**, **f**: OS MasterMap and **g**, **h**, **i**: the results of the presented methodology.

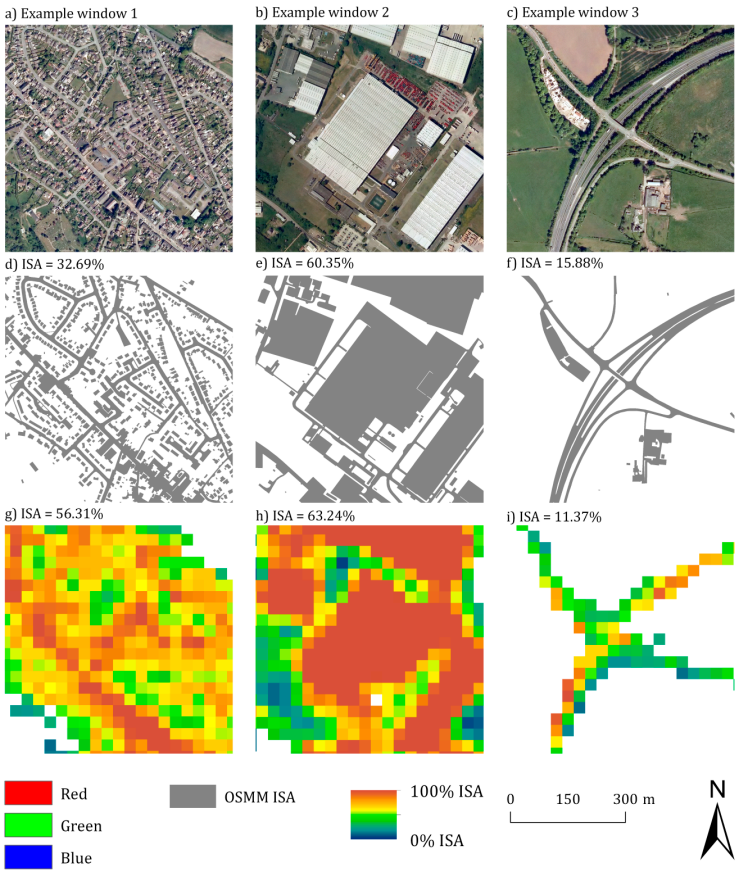

The performance of both datasets compared well with the high resolution area photography in areas of industrial land use and areas of minimal ISA, such as roads (Figure 7). When an unsupervised, *Nearest Neighbour* classification was performed on the three example windows (Table 3), this was clearly shown in the percentage of ISA in each window.

Table 3. Percentage of ISA in each example window (from Figure 6) where Classifier is the result of the methodology presented in this paper, OSMM is the OS MasterMap product, and AP is the result of the nearest neighbour classification on the high resolution aerial photography.

Example Window (Figure 7)	Classifier	OSMM	AP
1	56.31	32.69	50.29
2	63.24	60.35	62.84
3	11.37	15.88	13.61

When analysing the skipped areas of ISA from the OS MasterMap, it was revealed that around 50% of these areas were small dispersed minor roads, while the other 50% were predominantly farm buildings/yards and hard standings. While example Windows 1 and 2 slightly overestimated (falsely classified) ISA, Window 3 illustrates the masking of farm buildings/ yards and hard standings in the 1st part of the classification with the small underestimation of ISA. Overestimation in the examples may be accounted for while considering the weather conditions of the acquisition date with high radiation values produced from clear skies in the visible light channels.

5.3. Limitations and Recommendations

As the findings of this study suggested, much of the underestimated/skipped ISA is resultant from minor roads and farm infrastructure. While the former is not resolvable while using the Landsat archive, given the resolution, the latter can be resolved by filtering the masking LPIS polygons to include farm buildings/yards and other concrete surfaces, for further analysis. This will enable the inclusion of these areas within study site ISA estimations. While the impact of this on pixels containing ISA, may be significant (~20% more), impact on ISA estimations is not predicted to be. However, to gain a thorough estimation over a national scale, to which the methodology is intended to be extended, the authors suggest that this is a necessary improvement for future iterations of the methodology. Due to the limited frequency of 100% cloud free data from Landsat satellites over Wales and the UK, a yearly report of ISA was unable to be achieved in the instance of this study. The replacement of cloud-tainted data is achievable through the method proposed by [32], and performed to an extremely high level. However, this was not achievable on a perennial base. A recommendation to resolve this would be to conduct the estimation of ISA over a number of years. With most national reporting conducted on a bi-quinquennial basis, it is acceptable within a policy context that the methodology is also carried out on the same temporal scale. [45], the integration of land surface temperature and LSMA-derived fraction images, creates an effective tool for the refinement of a high-quality impervious surface image. In future iterations of the methodology, moving towards the proposed bi-quinquennial cycle, land surface temperature may therefore be key for further success and greater levels of accuracy.

Finally there were a small number of underestimations in ISA highlighted in Figure 6, towards the higher percentages. This is due, to the removal of potential ISA by overhanging vegetation; a side effect of the leaf on capture period of the high resolution aerial photography [76]. For future study, it is suggested that this be addressed by utilizing leaf off imagery where possible and therefore correcting for this. For the overestimations in the lower percentages, it is suggested that this is due to the misclassification of some large areas of railway track within the assessment windows. In future iterations of the methodology, ancillary data identifying railway tracks would remedy this problem.

6. Conclusions

In this study, a combination of methods was proposed for mapping ISA based on freely distributed Earth Observation (EO) imagery by combining a traditional classifier and a linear spectral mixture analysis (LSMA). The usefulness of the proposed technique in mapping ISA was demonstrated for several regions in Wales, UK using a series of Landsat TM/ETM+ images to extract ISA over these study sites.

With the continuation of the Landsat programme, the protraction of the proposed methodology has been assured. The new sensor also has superior facilities for detecting clouds in the sub-blue wavelengths. These areas may then be replaced by other frequently repeated scenes and a full classification of the study area can be achieved. The inclusion of other data, such as Synthetic Aperture Radar (SAR) may both further improve the accuracy of the current technique and lead to a more detailed classification hierarchy. Finally, the present study not only inaugurates the local retrieval of ISA for Wales, but also meliorates the existing EU international figures, and expands relatively stationary "global" US/China centric ISA research. The practical usefulness of the method proposed here remains to be seen in the near future.

Acknowledgments

Authors gratefully acknowledge the United Stated Geological Survey (USGS) for providing free access to the Landsat TM satellite images. Authors would also like to thank the colleagues at the Welsh Government who assisted and supported the development of this research work.

Author Contributions

Douglas Scott and George P. Petropoulos conceived and designed the methodology; Douglas Scott performed the methodology and analyzed the data; Janet Moxley and Heath Malcolm contributed to the discussion and conclusion sections; Douglas Scott wrote the paper; George P. Petropoulos contributed to the manuscript preparation, writing and revision.

Conflicts of Interest

The authors declare no conflict of interest.

References

1. Kunzig, R. Population 7 billion. *Natl Geogr.* **2011**, *219*, 32–63.

2. Webb, N.; Broomfield, M.; Cardenas, L.; MacCarthy, J.; Murrells, T.; Pang, Y.; Passant, N.; Thistlewaite, G.; Thomson, A. *UK Greenhouse Gas Inventory, 1990 to 2011: Annual Report for Submission under the Framework Convention on Climate Change*; Ricardo-AEA: Didcot, Oxfordshire, UK, 2013; p. 816.
3. Arnold, C.L.; Gibbons, C.J. Impervious surface coverage: The emergence of a key environmental indicator. *J. Am. Plan. Assoc.* **1996**, *62*, 243–258.
4. Hasse, J.E.; Lathrop, R.G. Land resource impact indicators of urban sprawl. *Appl. Geogr.* **2003**, *23*, 159–175.
5. Lee, S.; Lathrop, R.G. Subpixel analysis of Landsat ETM+ using self-organizing map (SOM) neural networks for urban land cover characterization. *IEEE Trans. Geosci. Remote Sens.* **2006**, *44*, 1642–1654.
6. Yang, F.; Matsushita, B.; Yang, W.; Fukushima, T. Mapping the human footprint from satellite measurements in Japan. *ISPRS J. Photogramm. Remote Sens.* **2014**, *88*, 80–90.
7. Seto, K.C.; Güneralp, B.; Hutyra, L.R. Global forecasts of urban expansion to 2030 and direct impacts on biodiversity and carbon pools. *PNAS* **2012**, *109*, 16083–16088.
8. Blaschke, T. Object based image analysis for remote sensing. *ISPRS J. Photogramm. Remote Sens.* **2010**, *65*, 2–10.
9. Blaschke, T.; Strobl, J. What's wrong with pixels? Some recent developments interfacing remote sensing and GIS. *GeoBIT/GIS* **2001**, *6*, 12–17.
10. Borak, J. S.; Strahler, A.H. Feature selection and land cover classification of a MODIS-like data set for a semiarid environment. *Int. J. Remote Sens.* **1999**, *20*, 919–938.
11. Mathur, A.; Foody, G.M. Crop classification by support vector machine with intelligently selected training data for an operational application. *Int. J. Remote Sens.* **2008**, *29*, 2227–2240.
12. Petropoulos, G.P.; Partsinevelos, P.; Mitraka, Z. Change detection of surface mining activity and reclamation based on a machine learning approach of multi-temporal Landsat TM imagery. *Geocarto Int.* **2013**, *28*, 323–342.
13. Weng, Q. *Remote Sensing of Impervious Surfaces*; CRC Press: Boca Raton, FL, USA, 2010.
14. Frauman, E.; Wolff, E. Segmentation of very high spatial resolution satellite images in urban areas for segments-based classification. In Proceedings for 3rd International Symposium Remote Sensing and Data Fusion Over Urban Areas, Tempe, AZ, USA, 14–16 March 2005.
15. Shackleford, A.K.; Davis, C.H. A combined fuzzy pixel-based and object-based approach for classification of high-resolution multispectral data over urban areas. *IEEE Trans. Geosci. Remote Sens.* **2003**, *41*, 2354–2363.
16. Yuan, F.; Bauer, M.E. Mapping impervious surface area using high resolution imagery: A comparison of object-based and per pixel classification. In Proceedings of ASPRS 2006 Annual Conference, Reno, NV, USA, 1–5 May 2006.
17. Petropoulos, G.P.; Vadrevu, K.P.; Kalaitzidis, C. Spectral angle mapper and object-based classification combined with hyperspectral remote sensing imagery for obtaining land use/cover mapping in a Mediterranean region. *Geocarto Int.* **2013**, *28*, 114–129.
18. Petropoulos, G. P.; Kalaitzidis, C.; Prasad Vadrevu, K. Support vector machines and object-based classification for obtaining land-use/cover cartography from Hyperion hyperspectral imagery. *Comput. Geosci.* **2012**, *41*, 99–107.

19. Weng, Q. Remote sensing of impervious surfaces in the urban areas: Requirements, methods, and trends. *Remote Sens. Environ.* **2012**, *117*, 34–49.
20. Ling, F.; Li, X.; Xiao, F.; Fang, S.; Du, Y. Object-based sub-pixel mapping of buildings incorporating the prior shape information from remotely sensed imagery. *Int. J. Appl. Earth Obs. Geoinf.* **2012**, *18*, 283–292.
21. Fankhauser, R. Automatic determination of imperviousness in urban areas from digital orthophotos. *Water Sci. Technol.* **1999**, *39*, 81–86.
22. Weng, Q. Modelling urban growth effects on surface runoff with the integration of remote sensing and GIS. *Environ. Manag.* **2001**, *28*, 737–748.
23. Dams, J.; Dujardin, J.; Reggers, R.; Bashir, I.; Canters, F.; Batelaan, O. Mapping impervious surface change from remote sensing for hydrological modelling. *J. Hydrol.* **2013**, *485*, 84–95.
24. Berezowski, T.; Chormanski, J.; Batelaan, O.; Canters, F.; Van de Vorde, T. Quantifying land-cover proportions for urban runoff prediction. The advantage of distributed remote sensing techniques. In Proceedings of EGU General Assembly 2012, Vienna, Austria, 22–27 April 2012.
25. Hu, X.; Weng, Q. Estimating impervious surfaces from medium spatial resolution imagery: A comparison between fuzzy classification and LSMA. *Int. J. Remote Sens.* **2011**, *32*, 5645–5663.
26. Weng, Q.; Rajasekar, U.; Hu, X. Modelling urban heat islands and their relationship with impervious surface and vegetation abundance by using ASTER images. *IEEE Trans. Geosci. Remote Sens.* **2011**, *49*, 4080–4089.
27. Liu, H.; Weng, Q. Landscape metrics for analysing urbanization-induced land use and land cover changes. *Geocarto Int.* **2013**, *28*, 582–593.
28. Quarmby, N.A.; Cushine, J.L. Monitoring urban land cover changes at the urban fringe from SPOT HRV imagery in south-east England. *Int. J. Remote Sens.* **1989**, *10*, 953–963.
29. Fuller, R.M.; Groom, G.B.; Jones, A.R. The land cover map of Great Britain: An automated classification of Landsat Thematic Mapper data. *Photogramm. Eng. Remote Sens.* **1994**, *60*, 553–562.
30. Grey, W.M.F.; Luckman, A.J.; Holland, D. Mapping urban change in the UK using satellite radar interferometry. *Remote Sens. Environ.* **2003**, *87*, 16–22.
31. Kampouraki, M.; Wood, G.A.; Brewer, T. The application of remote sensing to identify and measure sealed areas in urban environments. Proceeding from ISPRS 1st International Conference on Object-Based Image Analysis (OBIS 2006), Salzburg, Austria, 4–5 July 2006.
32. Martinuzzi, S.; Gould, W.A.; González, O.M.R. *Creating Cloud-Free Landsat ETM+ Data Sets in Tropical Landscapes: Cloud and Cloud-Shadow Removal*; IITF-GTR-32; U.S. Department of Agriculture, Forest Service, International Institute of Tropical Forestry: Portland, OR, USA, 2007.
33. Gurney, C.M. The use of contextual information to detect cumulous clouds and cloud shadow in Landsat data. *Int. J. Remote Sens.* **1982**, *3*, 51–62.
34. Irish, R. Landsat 7 automatic cloud cover assessment. *Proc. SPIE* **2000**, *4049*, 348–355.
35. Irish, R.; Barker, J.; Goward, S.; Arvidson, T. Characterization of the Landsat-7 ETM+ automated cloud-cover assessment (ACCA) algorithm. *Photogramm. Eng. Remote Sens.* **2006**, *72*, 1179–1188.
36. Wang, B.; Ono, A.; Muramatsu, K.; Fujiwara, N. Automated detection and removal of clouds and their shadows from Landsat TM images. *IEICE Trans. Inf. Syst.* **1999**, *E82-D*, 453–460.
37. Zhu, Z.; Woodcock, C.E. Object-based cloud and cloud shadow detection in Landsat imagery. *Remote Sens. Environ.* **2012**, *118*, 83–94.

38. Jin, S.; Homer, C.; Yang, L.; Xian, G.; Fry, J.; Danielson, P.; Townsend, P.A. Automated cloud and shadow detection and filling using two-date Landsat imagery in the USA. *Int. J. Remote Sens.* **2012**, *34*, 1540–1560.
39. Goodwin, N.R.; Collett, L.J.; Denham, R.J.; Flood, N.; Tindall, D. Cloud and cloud shadow screening across Queensland Australia: An automated method for Landsat TM/ETM+ time series. *Remote Sens. Environ.* **2013**, *134*, 50–65.
40. Li, D.; Tang, P. A sensor specified method based on spectral transformation for masking cloud in Landsat data. *IEEE J. Sel. Top. Appl. Earth Obs. Remote Sens.* **2013**, *6*, 1619–1627.
41. Small, C. Estimation of urban vegetation abundance by spectral mixture analysis. *Int. J. Remote Sens.* **2001**, *22*, 1305–1334.
42. Phinn, S.; Stanford, M.; Scarth, P.; Murray, A.T.; Shyy, P.T. Monitoring the composition of urban environments based on the vegetation-impervious surface-soil (VIS) model by subpixel analysis techniques. *Int. J. Remote Sens.* **2002**, *23*, 4131–4153.
43. Wu, C.; Murray, A.T. Estimating impervious surface distribution by spectral mixture analysis. *Remote Sens. Environ.* **2003**, *84*, 493–505.
44. Song, C. Spectral mixture analysis for subpixel vegetation fractions in the urban environment: How to incorporate endmember variability? *Remote Sens. Environ.* **2005**, *95*, 248–263.
45. Lu, D.; Weng, Q. Use of impervious surface in urban land-use classification. *Remote Sens. Environ.* **2006**, *102*, 146–160.
46. Lu, D.; Moran, E.; Hetrick, S. Detection of impervious surface change with multitemporal Landsat images in an urban-rural frontier. *ISPRS J. Photogramm. Remote Sens.* **2011**, *66*, 298–306.
47. Lu, D.; Li, G.; Moran, E.; Batistella, M.; Freitas, C. Mapping impervious surfaces with the integrated use of Landsat Thematic Mapper and radar data: A case study in an urban-rural landscape in the Brazillian Amazon. *ISPRS J. Photogramm. Remote Sens.* **2011**, *66*, 798–808.
48. Ridd, M.K. Exploring a VIS (vegetation-impervious surface-soil) model for urban ecosystem analysis through remote sensing: Comparative anatomy for cities. *Int. J. Remote Sens.* **1995**, *16*, 2165–2185.
49. Hu, X.; Weng, Q. Estimating impervious surfaces from medium spatial resolution imagery using the self-organizing map and multi-layer perception neural networks. *Remote Sens. Environ.* **2009**, *113*, 2089–2102.
50. Lee, S.; Lathrop, R.G. Sub-pixel estimation of urban land cover components with linear mixture model analysis and Landsat Thematic Mapper imagery. *Int. J. Remote Sens.* **2005**, *26*, 4885–4905.
51. Jones, P.S.; Stevens, D.P.; Blackstock, T.H.; Burrows, C.R.; Howe, E.A. *Priority Habitats of Wales: A Technical Guide*; Countryside Council for Wales: Bangor, UK, 2003.
52. Joint Nature Conservation Committee. *Handbook for Phase 1 Habitat Survey—A Technique for Environmental Audit*; Joint Nature Conservation Committee: Peterborough, UK, 2010.
53. Revell, P.; Regnauls, N.; Thom, S. Generalising OS MasterMap® topographic buildings and ITN road centerlines to 1:50000 scale using a spatial hierarchy of agents, triangulation and topology. In Proceedings of the International Cartographic Conference, A Coruna, Spain, 9–16 July 2005.
54. Smith, G.B.; Boyd, M.; Downs, M.; Gregory, T.; Morton, M.; Brown, D.; Thomson, N.A. UK land cover map production through the generalisation of OS MasterMap®. *Cartogr. J.* **2007**, *44*, 276–283.

55. Thomson, M.K. Dwelling on Ontology-Semantic Reasoning over Topographic Maps. Ph.D. Thesis, University College London, London, UK, 2009.
56. Kuntz, S.; Schmeer, E.; Jochum, M.; Smith, G. Towards an European land cover monitoring service and high-resolution layers. In *Land Use and Land Cover Mapping in Europe*; Manakos, I., Braun, M., Eds.; Springer: Dordrecht, The Netherlands, 2014; pp. 43–52.
57. Lefebvre, A.; Beaugendre, N.; Pennec, A.; Sannier, C.; Corpetti, T. Using data fusion to update built-up areas of the 2012 European High-Resolution Layer Imperviousness. In Proceedings of the 33rd EARSeL Symposium Conference, Matera, Italy, 3–6 June 2013; pp. 321–328.
58. Lucas, R.; Medcalf, K.; Brown, A.; Bunting, P.; Breyer, J.; Clewley, D.; Keyworth, S.; Blackmore, P. Updating the Phase 1 habitat map of Wales, UK, using satellite sensor data. *ISPRS J. Photogramm. Remote Sens.* **2011**, *66*, 81–102.
59. Baxter, R.; Lees, L. The rebirth of high-rise living in London: Towards a sustainable, inclusive, and liveable urban form. In *Regenerating London: Governance, Sustainability and Community in a Global City*; Routledge: London, UK, 2009; pp. 151–172.
60. Teh, H.T.; Lim, H.S.; Matjafri, M.Z. Deriving urban sealed surface density map using linear spectral unmixing analysis. In Proceedings of 2011 IEEE International Conference on Space Science and Communication (IconSpace), Penang, Malaysia, 12–13 July 2011.
61. Zhu, S.; Zhang, G. Analysis on relationship between urban land surface temperature and landcover from Landsat ETM+ data. In Proceedings of 2011 Fourth International Symposium on Knowledge Acquisition and Modeling (KAM), Sanya, China, 8–9 October 2011.
62. Sagris, V.; Devos, W. *LPIS Core Conceptual Model: Methodology for Feature Catalogue and Application Schema*; Joint Research Centre: Ispra, Italy, 2008.
63. Deng, C.; Wu, C. BCI: A biophysical composition index for remote sensing of urban environments. *Remote Sens. Environ.* **2012**, *127*, 247–259.
64. Settle, J.J.; Drake, N.A. Linear mixing and the estimation of ground cover proportions. *Int. J. Remote Sens.* **1993**, *14*, 1159–1177.
65. Kauth, R.J.; Thomas, G.S. The tasselled cap—A graphic description of the spectral-temporal development of agricultural crops as seen by Landsat. In Proceedings of the Symposium on Machine Processing of Remotely Sensed Data, West Lafayette, IN, USA, 29 June–1 July 1976.
66. Huang, C.; Wylie, B.; Yang, L.; Homer, C.; Zylstra, G. Derivation of a tasselled cap transformation based on Landsat 7 at-satellite reflectance. *Int. J. Remote Sens.* **2002**, *23*, 1741–1748.
67. Congalton, R.G. A review of assessing the accuracy of classifications of remotely sensed data. *Remote Sens. Environ.* **1991**, *37*, 35–46.
68. Congalton, R.G.; Green, K. *Assessing the Accuracy of Remotely Sensed Data: Principles and Practices*, 2nd ed.; CRC Press: Boca Raton, FL, USA, 2008.
69. Foody, G.M. Status of land cover classification accuracy assessment. *Remote Sens. Environ.* **2002**, *80*, 185–201.
70. Bauer, M.E.; Loffelholz, B.C.; Wilson, B. Estimating and mapping impervious surface area by regression analysis of Landsat imagery. In *Remote Sensing of Impervious Surfaces*; Weng, Q., Ed.; Taylor & Francis Group: Boca Raton, FL, USA, 2008; pp. 31–47.
71. Wu, C. Normalized spectral mixture analysis for monitoring urban composition using ETM+ imagery. *Remote Sens. Enviorn.* **2004**, *93*, 480–492.

72. Kontoes, C.C.; Poilve, H.; Florsch, G.; Keramitsoglou, I.; Paralikidis, S. A comparative analysis of a fixed thresholding *vs.* a classification tree approach for operational burn scar detection and mapping. *Int. J. Appl. Earth Obs. Geoinf.* **2009**, *11*, 299–316.
73. Petropoulos, G.P.; Kontoes, C.C.; Keramitsoglou, I. Land cover mapping with emphasis to burnt area delineation using co-orbital ALI and Landsat TM imagery. *Int. J. Appl. Earth Obs. Geoinf.* **2012**, *18*, 344–355.
74. Dallimer, M.; Tang, Z.; Bibby, P.R.; Brindley, P.; Gaston, K.J.; Davies, Z.G. Temporal changes in greenspace in a highly urbanized region. *Biol. Lett.* **2011**, *7*, 763–766.
75. Smith, G.M. Land use & land cover mapping in Europe: Examples from the UK. In *Land Use and Land Cover Mapping in Europe*, 1st ed.; Manakos, I., Braun, M., Eds.; Springer: Dordrecht, The Netherlands, 2014; pp. 273–282.
76. Jones, J.W.; Jarnagin, T. Evaluation of a moderate resolution, satellite-based impervious surface map using an independent, high-resolution validation data set. *J. Hydrol. Eng.* **2009**, *14*, 369–376.